Supporting Information:

High-throughput, non-equilibrium studies of single biomolecules using glass made nanofluidic devices

Mattia Fontana[1,#], Carel Fijen[1,#], Serge G. Lemay[2], Klaus Mathwig[2,3*], and Johannes Hohlbein[1,4*]

[1] Wageningen University and Research, Laboratory of Biophysics, Stippeneng 4, Wageningen, 6708 WE, The Netherlands

[2] University of Twente, MESA+ Institute for Nanotechnology, P.O. Box 217, Enschede, 7500 AE, The Netherlands

[3] University of Groningen, Groningen Research Institute of Pharmacy, Pharmaceutical Analysis, P.O. Box 196, 9700 AD, Groningen, The Netherlands

[4] Wageningen University and Research, Microspectroscopy Research Facility, Stippeneng 4, Wageningen, 6708 WE, The Netherlands

[#] These authors contributed equally to this work.

* To whom correspondence should be addressed:

K.M.; Tel.: +31 50 363 3022; Email: k.h.mathwig@rug.nl;

J.H.; Tel.: +31 317 482 635; Email: johannes.hohlbein@wur.nl

Keywords: Nanochannel, nanofluidic mixing, fluorescence detection, single molecules, FRET

Overview

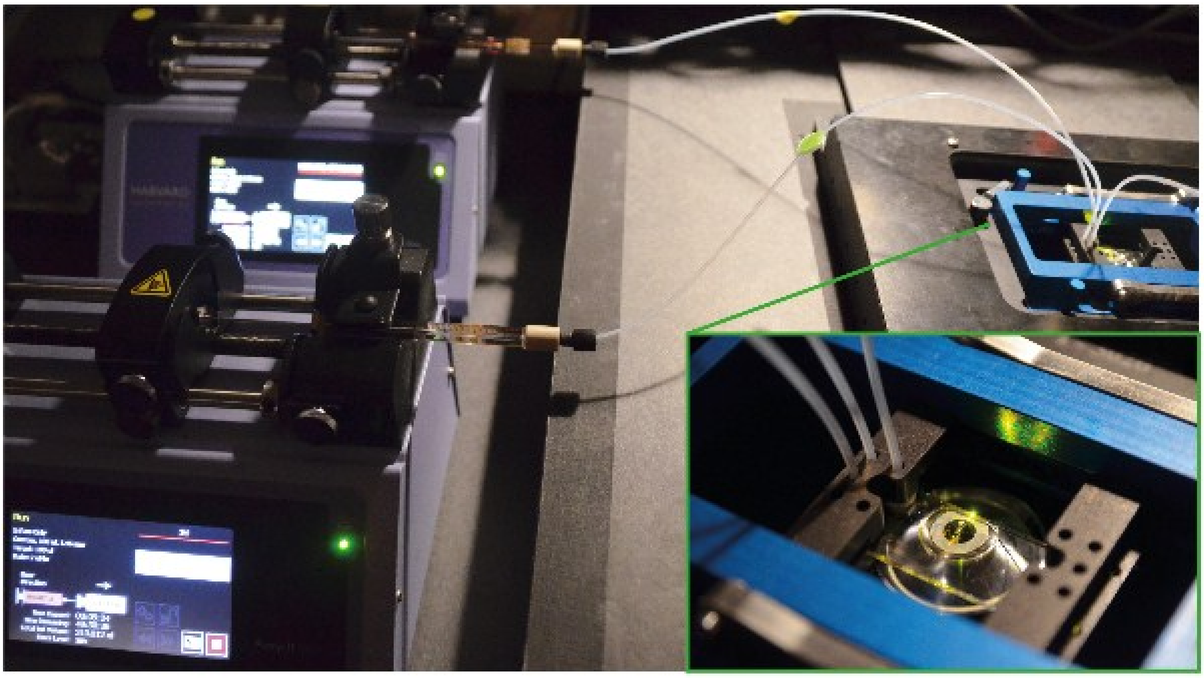

Fig. S1 Overview of the fluidic setup on a home-built microscope.

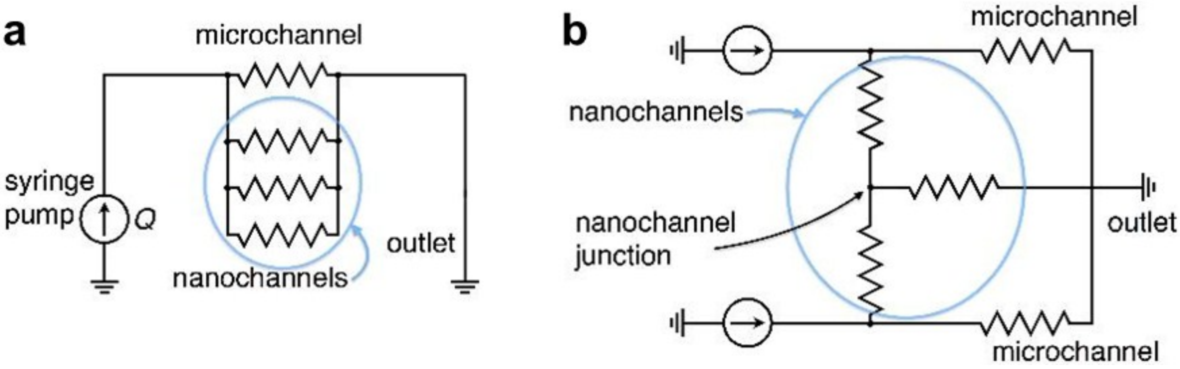

Fig. S2 Equivalent circuit diagram of the nano-/microfluidic channel geometries. Syringe pumps act as current sources delivering constant flow rates *Q* and channels oppose flow by a hydraulic resistance R_{hyd} (**a**) Parallel flow configuration of a bypassing microchannel and a nanochannel array. (**b**) Diagram of a micro-/nanofluidic mixing circuit. Here, reaction products are imaged at and downstream the nanochannel junction.

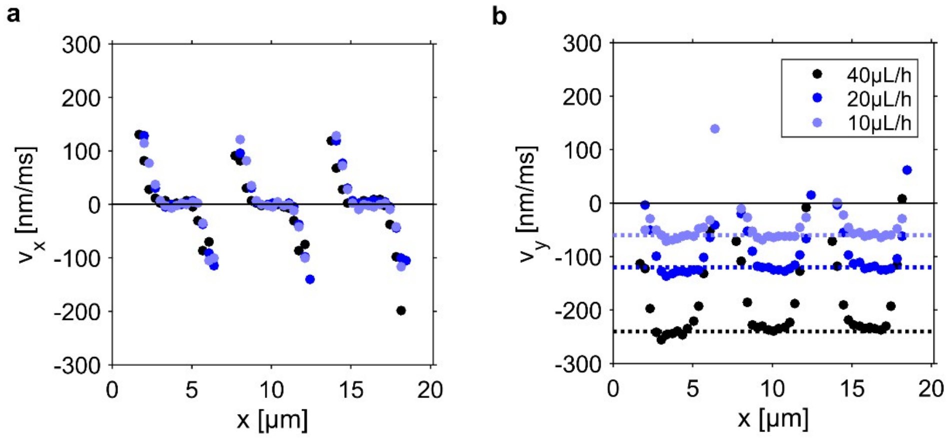

Fig. S3 Experimental flow velocity profiles for different pump rates in three parallel nanochannels (40, 20, and 10 µL/h). (**a**) Velocity profiles along *x*: this direction is orthogonal to the applied flow thus the profiles are not influenced by the pump rate and are averaged around zero. The negative and positive velocities at the edges of each nanochannels arise from the border effect, in which a molecule very close to the nanochannel wall cannot diffuse further hence on average will diffuse back toward the central axis of the channel (**b**) Velocity profiles along *y*: Reference lines are drawn at (-60, -120 and -240 nm/ms). The flow speed registered inside the nanochannels scales linearly with the pump rate as expected for our system. All the profiles show a plateau for the velocity in the center of the channels (see also Fig. S4).

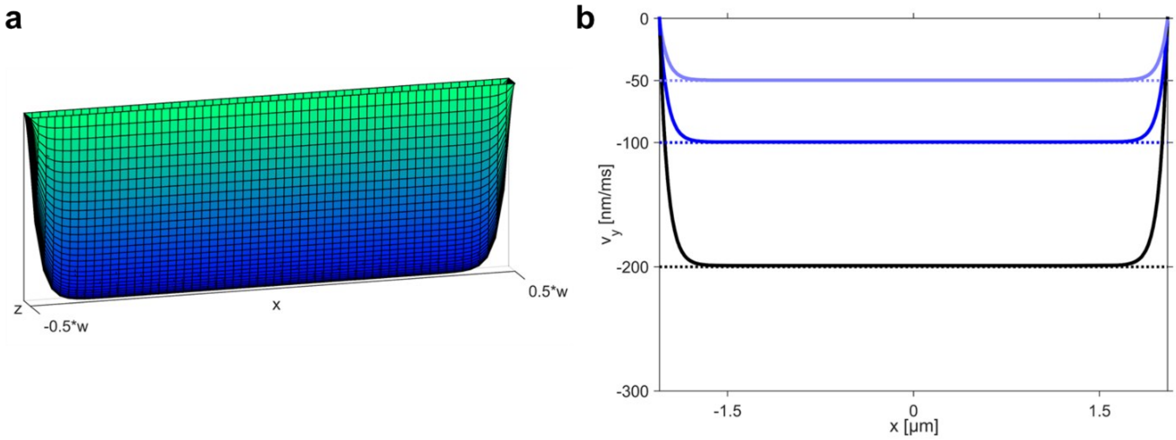

Fig. S4 Theoretical 3D and 2D velocity profiles (see also Supporting Note 2). (**a**) Theoretical 3D velocity surface for Poiseuille flow in a nanochannel. The velocity surface was calculated using the dimensions of one parallel nanochannel. Along the height of the channels (*z*, 0.2 µm) the velocity profile is parabolic. Along most of the width (*x*, here 4.1 µm) the flow speed is constant (parallel plate-like scenario). (**b**) Theoretical 2D velocity profiles for Poiseuille flow in a nanochannel. Theoretical velocity profiles calculated for different pump rates: 10, 20, and 40 µL/h; the value of the plateau velocity (v_{max}) scales linearly with the pump rate.

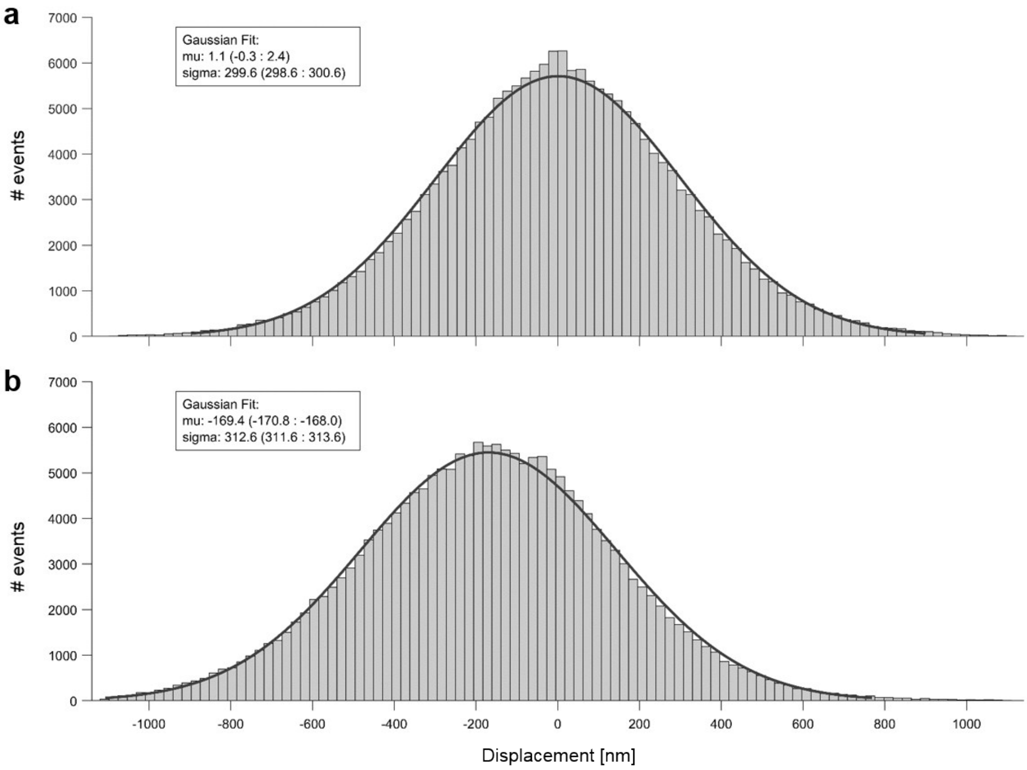

Fig. S5 Example of frame-wide displacement distributions. Bending sensor in absence of KF in parallel nanochannels at pump rate of 20 uL/h. The displacement distribution is a normal distribution with mean proportional to the flow applied on that direction and variance proportional to the diffusivity of the tracked species (see also Material and Methods). (**a**) The distribution along x is centered on zero since there is no flow along this direction. Note that the 95% interval of confidence for the mean (mu) contains the value 0. (**b**) The mean of the displacement distribution along y is shifted to -169.4 nm; this, given the 1.5 ms between the green and red laser excitation results in a mean velocity across the field of view of 112.9(9) nm/ms (95% interval of confidence on the mean).

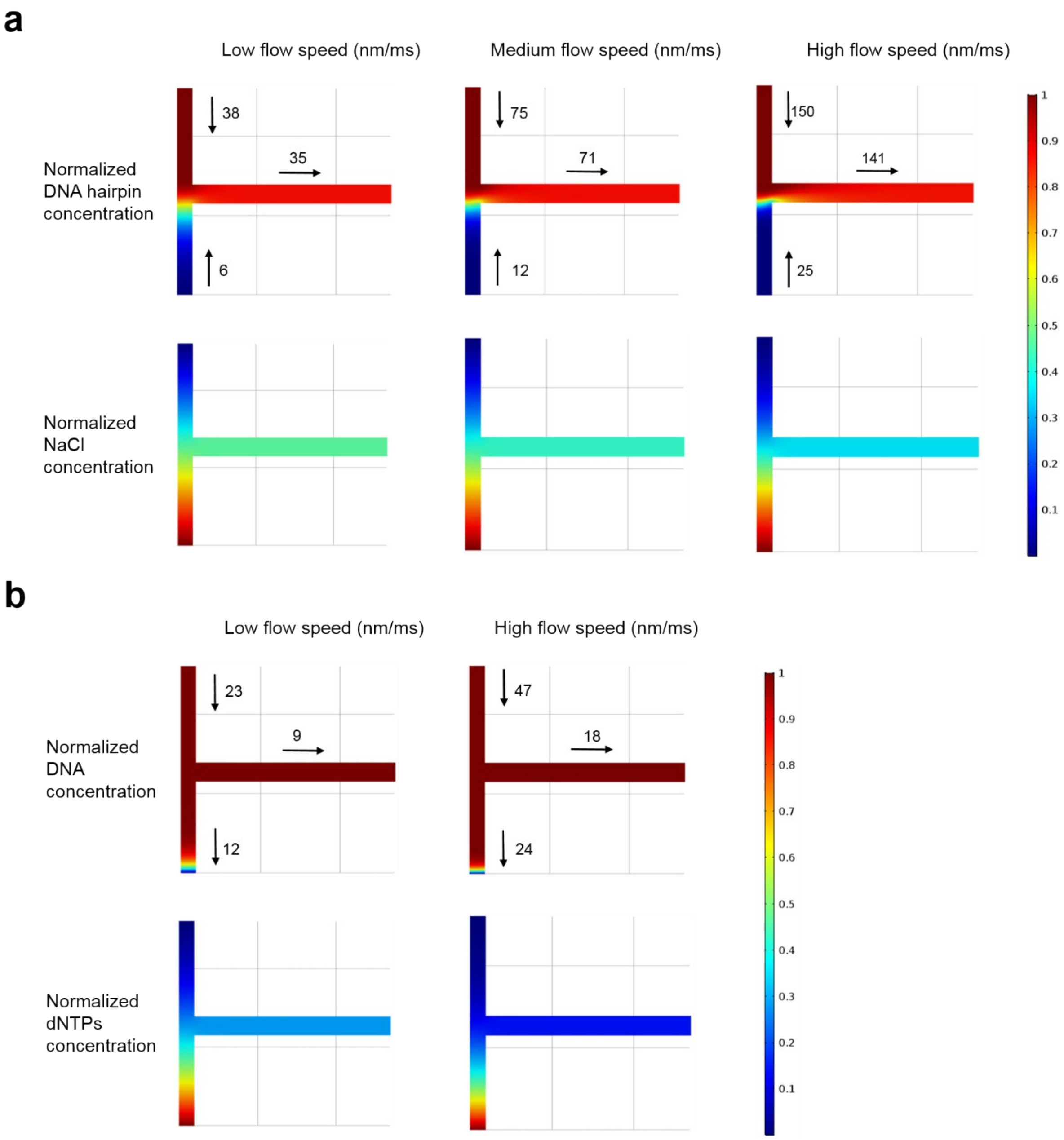

Fig. S6 Finite element simulations (COMSOL, see also Supporting Note 4). A three-dimensional geometry of inlet channels of combined 52 µm × 3.8 µm × 0.2 µm and a downstream outlet/observation channel of 50 µm × 4.7 µm × 0.2 µm was used. Concentration profiles in the center plane at *z* = 100 nm are shown. (**a**) Simulations of the DNA hairpin experiment in the mixing nanochannels. The simulated flow velocities for the three tested pump settings are reported. The experimentally obtained value for the diffusion coefficient of the hairpin was used (35 µm^2/s), together with an approximate value for the diffusion coefficient of salt (2000 µm^2/s). (**b**) Simulation of the DNA polimerization experiment. The simulated flow velocities for the two tested flow rates are reported. The experimentally obtained value for the diffusion coefficient of the DNA was used (25 µm^2/s), together with an approximate value for the diffusion coefficient of the dNTPs (400 µm^2/s).

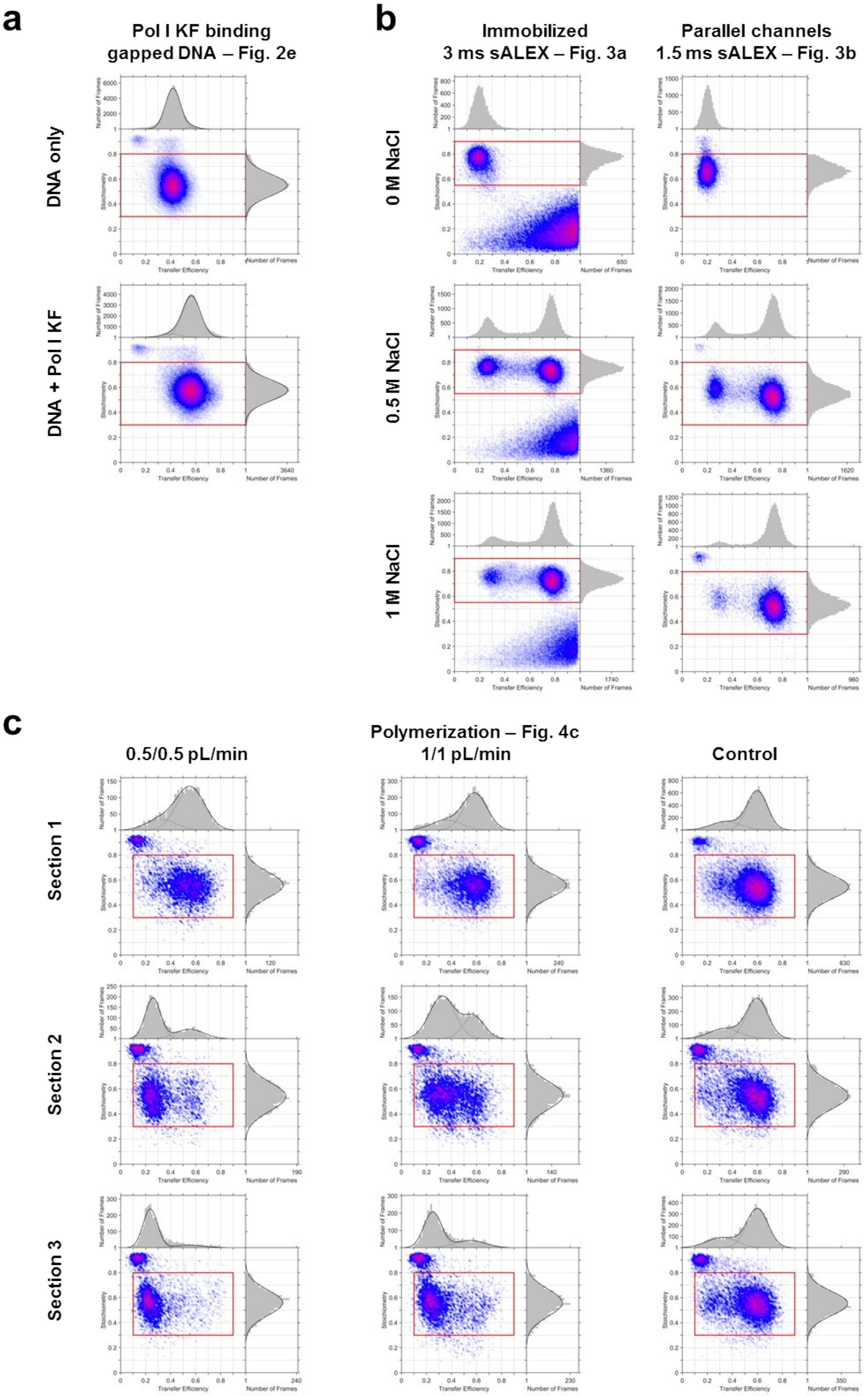

Fig S7. *E**/S histograms of data shown in Figs 2e, 3a and 4. Only data inside the red box is projected on the axes. FRET efficiency *E** is on the x-axis, stoichiometry S is on the y-axis.

Supporting Note 1: Achieving parallel control

Flow was driven by syringe pumps (Pump 11 Pico Plus Elite; Harvard Apparatus, USA). In Parallel Flow Control (PFC), low flow rates are achieved by dividing the syringe flow rate *Q* into the microchannel and nanochannels according to the channels' hydraulic resistance, which is calculated as[1,2]

$$R_{\text{hyd}} \approx \frac{12\eta L}{1 - 0.630\left(\frac{h}{w}\right)} \cdot \frac{1}{h^3 w} \text{ for } h < w. \qquad (1)$$

Here, η is the dynamic viscosity of 0.001 Pa s in water and *h*, *w* and *L* are the height, width and length of a nanochannel, respectively (A pressure Δp across a channel drops according to the Hagen Poiseuille Law $Q = \Delta p / R_{\text{hyd}}$, and for parallel resistances $R_{\text{array}} = 1/\sum R_{\text{hyd, i}}^{-1}$ applies.). Due to the cubic dependence h^3, the flow rate in each nanochannel is strongly reduced compared to the microchannel.

For high flow rate of 20 pL/min inside one nanochannel of the parallel design, the pump generates a pressure of about 15 kPa while operating at 85 uL/h. This large ratio of flows allows the dead volume in the 1 mm wide and up to 2 cm long feeding microchannels (0.1 uL) to be replaced in seconds.

For the mixing device, two syringe pumps deliver flow to both feeding nanochannel inlets (each 20 µm long, 3.8 µm wide and 200 nm high). A single nanochannel (100 µm long, 4.7 µm wide and 200 nm high) is positioned downstream of the junction. Two bypassing microchannels lead to an overall reduction factor of 140.000 of the nanochannel flow compared to the combined microchannel flows.

We note that a geometry similar to the one of our parallel devices, where narrow channels are flanked with wide channels has been previously used in literature to achieve a different goal: maintain hydrostatic equilibrium between reservoirs connected by the channels.[3,4] Any small difference in hydrostatic pressure between the two reservoirs would be rapidly equilibrated through the wide channels; at the same time, thanks to the high reduction factor of this geometry the flow induced in the narrow channels would stay negligible, allowing to perform experiment where this condition is required.

Supporting Note 2: Poiseuille flow in rectangular nanochannels

The velocity for Poiseuille flow in our nanochannel geometry can be calculated using (reviewed in refererence[1])

$$v_y(x,z) = \frac{4h^2 \Delta p}{\pi^3 \eta L} \sum_{n.odd}^{\infty} \frac{1}{n^3} \left[1 - \frac{\cosh\left(n\pi \frac{x}{h}\right)}{\cosh\left(n\pi \frac{w}{2h}\right)} \right] \sin\left(n\pi \frac{z}{h}\right). \qquad \text{(S2)}$$

Here, Δp is the pressure difference between the two ends of the channels, η is the dynamic viscosity of the fluid, and *h*, *w* and *L* are the height, width and length of a nanochannel, respectively. The resulting flow surface (Fig. S5a) shows a central velocity plateau along most of the width (*x*) of the nanochannel whereas along the height (*z*) a parabolic profile is present.

While taking a movie of molecules flowing through the nanochannels we are acquiring the projection of the position of the particles in the *x,y*-plane; still, particle speed will also be a function of height. By calculating the displacements on the plane, we are neglecting the position of the molecule along *z* and the velocity profiles obtained in this way will therefore represent the velocity averaged along *z*:

$$v_y(x) = \frac{1}{h}\int_0^h v_y(x,z)dz \qquad \text{(S3)}$$

Using this equation, it is possible to calculate the expected velocity profile as seen in our experiments (see Fig. S5b).

Supporting Note 3: Finite element simulations

Three-dimensional finite element modeling (COMSOL Multiphysics 5.2a) was employed to determine steady-state concentration profiles of the different species. The geometry consists a T-shaped channel with a top segment of 52 μm × 3.8 μm × 0.2 μm connected to downstream channel of segment 50 μm × 4.7 μm × 0.2 μm as shown in Figure S6. A laminar flow profile was determined by solving the Stokes equations for an incompressible fluid:

$$\vec{\nabla}p = \eta\nabla^2\vec{v}, \quad \vec{\nabla}\cdot\vec{v} = 0. \qquad \text{(S7)}$$

As boundary conditions, inflow velocities as indicated in Figure S6, an outlet exit pressure 0 Pa, and no-slip conditions for all other boundaries were chosen. The calculated flow profile $\vec{v}$ was used to evaluate drift diffusion equations

$$\vec{v}\cdot\vec{\nabla}c_i = D_i\nabla^2 c_i \qquad \text{(S8)}$$

where c_i and D_i are the concentration and diffusivities of DNA hairpin, salt, DNA and dNTP as defined in the caption of Figure S6. We chose boundary conditions of *c*(DNA hairpin) = 1 mM and *c*(salt) = 0 mM at the right/upper inlet and of *c*(DNA hairpin) = 0 mM and *c*(salt) = 1 mM for the left/lower inlet. For mixing in the polymerization experiment we chose *c*(DNA) = 1 mM and *c*(dNTP) = 0 mM at the right/upper inlet and of *c*(DNA) = 0 mM and *c*(dNTP) = 1 mM at the left/lower inlet, respectively.

References

1 H. Bruus, *Lab. Chip*, 2011, **11**, 3742–3751.

2 K. Mathwig and S. G. Lemay, *Electrochimica Acta*, 2013, **112**, 943–949.

3 S. Pagliara, S. L. Dettmer, K. Misiunas, L. Lea, Y. Tan and U. F. Keyser, *Eur. Phys. J. Spec. Top.*, 2014, **223**, 3145–3163.

4 K. Misiunas, S. Pagliara, E. Lauga, J. R. Lister and U. F. Keyser, *Phys. Rev. Lett.*, 2015, **115**, 038301.